Title

Genomic Instability Is Induced by Persistent Proliferation of Cells Undergoing Epithelial-to-Mesenchymal Transition

Journal

Cell Reports, 17(10)

ISSN

2639-1856

Authors

Comaills, Valentine
Kabeche, Lilian
Morris, Robert
et al.

Publication Date

2016-12-01

DOI

10.1016/j.celrep.2016.11.022

HHS Public Access

Author manuscript

Cell Rep. Author manuscript; available in PMC 2017 December 06.

Published in final edited form as:

Cell Rep. 2016 December 06; 17(10): 2632–2647. doi:10.1016/j.celrep.2016.11.022.

Genomic Instability Is Induced by Persistent Proliferation of Cells Undergoing Epithelial-to-Mesenchymal Transition

Valentine Comaills[1,2], **Lilian Kabeche**[1], **Robert Morris**[1], **Rémi Buisson**[1], **Min Yu**[1,±], **Marissa Wells Madden**[1], **Joseph A. LiCausi**[1], **Myriam Boukhali**[1], **Ken Tajima**[1,2], **Shiwei Pan**[1], **Nicola Aceto**[1,$], **Srinjoy Sil**[1], **Yu Zheng**[1,3], **Tilak Sundaresan**[1,4], **Toshifumi Yae**[1,2], **Nicole Vincent Jordan**[1,3], **David T. Miyamoto**[1,4], **David T. Ting**[1,4], **Sridhar Ramaswamy**[1,4], **Wilhelm Haas**[1,4], **Lee Zou**[1,5], **Daniel A. Haber**[1,3,4], and **Shyamala Maheswaran**[1,2,#]

[1]Massachusetts General Hospital Cancer Center, Harvard Medical School, Charlestown, MA, 02129, USA

[2]Department of Surgery, Harvard Medical School, Charlestown, MA 02129, USA

[3]Howard Hughes Medical Institute, Chevy Chase, MD 20815, USA

[4]Department of Medicine, Charlestown, MA 02129, USA

[5]Department of Pathology, Harvard Medical School, Charlestown, MA 02129, USA

Summary

TGFβ secreted by tumor stroma induces Epithelial-to-Mesenchymal Transition (EMT) in cancer cells, a reversible phenotype linked to cancer progression and drug resistance. However, exposure to stromal signals may also lead to heritable changes in cancer cells, which are poorly understood. We show that epithelial cells failing to undergo proliferation arrest during TGFβ-induced EMT sustain mitotic abnormalities due to failed cytokinesis, resulting in aneuploidy. This genomic instability is associated with suppression of multiple nuclear envelope proteins implicated in mitotic regulation, and is phenocopied by modulating the expression of LaminB1. While TGFβ-induced mitotic defects in proliferating cells are reversible upon its withdrawal, the acquired genomic abnormalities persist, leading to increased tumorigenic phenotypes. In metastatic breast cancer patients, increased mesenchymal marker expression within single circulating tumor cells is

Address Correspondence to: Shyamala Maheswaran, Ph.D., MGH Cancer Center, Bldg 149, 13th Street, Charlestown, MA 02129, Maheswaran@helix.mgh.harvard.edu.

[±]Present address: Department of Stem Cell Biology and Regenerative Medicine, University of Southern California, Los Angeles, CA 90033, USA

[$]Present address: Department of Biomedicine, University of Basel, CH-4058 Basel, Switzerland

[#]Lead contact

Author Contributions

V.C. and S.M. conceived, designed and conducted the study, analyzed data and prepared the manuscript. D.A.H and L.Z. recommended experiments and edited manuscript. V.C., L.K, R.B. and M.W.M. performed most of the experiments. N.A., D.T.M., R. M. and S.R. performed bioinformatic and statistical analyses. M.B and W.H performed the proteomic data, S.S and D.T.T performed RNAseq. M. Y., N. A. and Y. Z. helped with in vivo experiments and cell line derivation, J.A.L, T.S., K.T. and T.Y. assisted with staining and enumeration. N. V. J. generated the human breast cancer associated fibroblasts used in this study.

correlated with genomic instability. These observations identify a mechanism whereby microenvironment-derived signals trigger heritable genetic changes within cancer cells contributing to tumor evolution.

Graphical Abstract

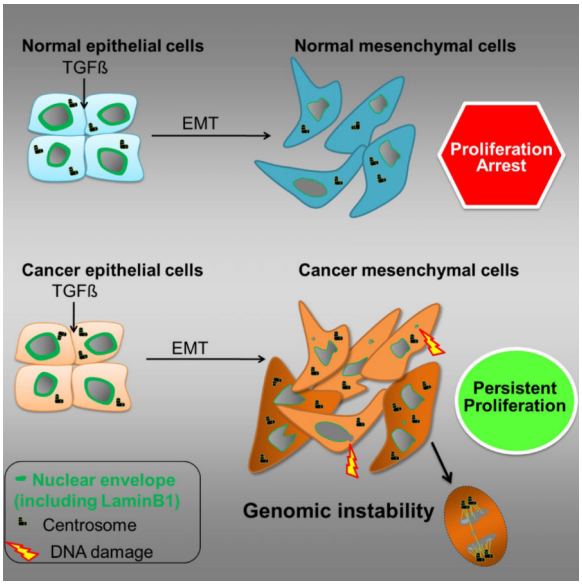

INTRODUCTION

EMT is a highly conserved developmental process that is aberrantly activated in epithelial cancer cells, inducing cell migration, stem-like characteristics and drug resistance (Nieto et al., 2016). The tight coregulation of growth arrest and EMT during physiological gastrulation is illustrated by studies in Drosophila and Xenopus, where induction of mitosis in cells undergoing EMT causes severe developmental defects (Grosshans and Wieschaus, 2000; Mata et al., 2000; Murakami et al., 2004; Seher and Leptin, 2000), suggesting that cell proliferation and EMT are generally incompatible. Unlike gastrulating cells in the embryo (Grosshans and Wieschaus, 2000; Mata et al., 2000; Murakami et al., 2004; Seher and Leptin, 2000), cancer cells undergoing EMT do not cease proliferation (Derynck et al., 2001; Massague, 2008). The functional consequences of persistent proliferation in epithelial cancer cells undergoing EMT have not been defined.

EMT is triggered by several secreted growth factors and cytokines constitutively present in the tumor microenvironment, and by a number of transcription factors (Nieto et al., 2016; Puisieux et al., 2014). Among these, TGFβ is noteworthy in being produced by tumor cells, reactive stromal cells as well as by platelets, which adhere to cancer cells when they invade into the bloodstream (Labelle et al., 2011; Massague, 2008; Yu et al., 2013). TGFβ has a complex role in tissue homeostasis: it inhibits the proliferation of normal epithelial cells but enhances metastasis through the induction of EMT in epithelial cancer cells, which are no longer sensitive to its growth inhibitory effects (Derynck et al., 2001; Massague, 2008).

The consequences of EMT in cancer cells remain the subject of debate. In mouse models, ectopic expression of master transcriptional regulators like Snail, Twist and Slug has major consequences for cellular invasiveness and tumorigenicity (Ocana et al., 2012; Ye et al., 2015). However, lineage tracing of epithelial and mesenchymal tumor cells within genetically engineered mice show that EMT may be dispensable for metastasis but contributes to drug resistance (Fischer et al., 2015; Maheswaran and Haber, 2015; Zheng et al., 2015). Chemotherapy-induced shifts between epithelial and mesenchymal states are also evident in “real time” within circulating tumor cells (CTCs) in the blood of breast cancer patients (Thiery and Lim, 2013; Yu et al., 2013). While the plasticity of EMT indicates that it is governed primarily by reversible changes in gene expression patterns (Nieto et al., 2016; Tam and Weinberg, 2013), it is unclear how these to contribute to fixed and heritable changes in tumor cells.

Here we show that TGFβ or SNAIL-induced EMT causes cytokinesis failure leading to mitotic defects. The appearance of these mitotic defects requires simultaneous cellular proliferation during EMT, and it is correlated with suppression of nuclear envelope proteins including LaminB1, which in addition to maintaining nuclear integrity have critical roles in mitosis (Gruenbaum and Foisner, 2015; Guttinger et al., 2009). EMT-induced mitotic abnormalities are reversible, but the inherited genomic instability persists and promotes tumorigenic phenotypes. The clinical significance of the link between EMT and genomic instability is supported by the prevalence of these defects within the mesenchymal population of CTCs in metastatic breast cancer patients. Together, our observations point to tumor microenvironment-derived signals that are capable of triggering heritable changes within adjacent cancer cells to enhance tumor progression.

RESULTS

TGFβ induces mitotic abnormalities

We evaluated the effect of TGFβ on MCF10A cells, which although considered ‘normal’ are immortalized mammary epithelial cells resistant to growth inhibition by TGFβ (Fig. S1A) (Kim et al., 2004; Soule et al., 1990). Treatment of MCF10A cells with 0.5 to 5 ng/mL TGFβ, conditions traditionally used to model EMT *in vitro*, increased the fraction of binucleated (BN) cells (Untreated: 0.81% ±0.71%; 5ng/mL TGFβ-treated: 11.3% ± 2.6%, $p<0.01$, Fig. 1A and S1A) and cells with micronuclei [(MN) (Untreated: 1.97% ±0.64%; 5ng/mL TGFβ-treated: 14.63% ±4.5%, $p<0.01$. Fig.1B and S1A)]. Removal of TGFβ decreased the number of BN cells (Fig. 1A), although MN persisted for longer periods of time (Fig. 1B). The nuclei in these BN cells were neither connected by a midbody nor were they phospho-histone H3-Ser10 positive (Fig. S1B, S1C), thus, they do not represent cells in the late telophase. Upon TGFβ treatment, MN with chromosomal fragments (MN C-) become more prevalent (Untreated: 0.47% ±0.18%; 5ng/mL 6 day-TGFβ-treated: 8.8% ± 0.84%, $p<0.01$) compared to chromosome-containing MN (MN C+; Untreated: 0.37% ±0.04%; 5ng/mL 6 day TGFβ-treated: 3.5% ± 0.42%, $p<0.01$) (Fig. 1C). TGFβ-induced mitotic abnormalities were also observed in the epithelial human breast cancer cell line SKBR3, and in the immortalized mouse mammary epithelial cell line, COMMA-D β-geo

[(CDβgeo) (Fig. S1D and S1E), neither of which undergo TGFβ-induced cell cycle arrest (Data not shown).

Using MCF10A cells expressing RFP-tagged histone H2B, we visualized TGFβ-induced mitotic anomalies in real time (Movie S1). Live imaging of TGFβ-treated RFP-H2B-MCF10A cells revealed cytokinesis failure resulting in BN cells and the appearance of MN (Fig. 1D, S2A, Movie S2). This is accompanied by nuclear blebbing and decreased in nuclear circularity, suggesting a possible defect in nuclear architecture involving lamins (Funkhouser et al., 2013); Fig. S2A]. The BN cells eventually divided (Fig. 1D, S2A, Movie S3). TGFβ increased the overall time for cell division, an effect reversible upon its withdrawal (Untreated: 51 ±16 min, TGFβ-treated: 116 ±86 min, post-TGFβ: 59 ±22 min, $p<0.0001$, Fig. 1E).

To better define the mechanism underlying these mitotic defects, we analyzed the first mitotic division in MCF10A cells following 24 hours of TGFβ treatment, and observed a 6-fold increase in BN cells (Untreated: 0.84±0.22%; TGFβ-24 hr: 5.33±0.18%). Nearly ~98.5±0.7% of these BN cells contained ≥ 3 centrosomes whereas only 2.55±0.22% of mononucleated cells contained ≥3 centrosomes (Fig. 1F). Evaluation of TGFβ-treated mitotic cells showed centrosome clustering and bipolar divisions (Fig. 1G), with none of the cells exhibiting multipolar division. This was accompanied by chromosome missegregation during anaphase (Fig. S2B) and increased mid-body bridge length (Fig. S2C). These results suggest that TGFβ primarily impairs cytokinesis resulting in BN cells with extra centrosomes, leading to chromosome missegregation (Ganem et al., 2009). The mitotic abnormalities decreased upon TGFβ withdrawal (Fig. 1G, S2B); mitotic cells with extra centrosomes were significantly higher following 3 days of TGFβ withdrawal compared to control cells, but gradually decreased suggesting that there might be selection bias against this population over time. Similar mitotic abnormalities were also observed in TGFβ-treated CDβgeo cells (Fig. S2D). Comet assays (Olive and Banath, 2006), a measure of DNA fragmentation within cells, revealed that TGFβ significantly increased DNA damage, which decreased upon TGFβ withdrawal (Fig. S2E; $p<0.005$).

TGFβ-induced mitotic abnormalities are dependent on EMT

To determine whether the TGFβ-induced mitotic defects are linked to EMT, we compared the time course of mitotic abnormalities with the shift in epithelial and mesenchymal markers. The emergence of BN and M-cells following TGFβ treatment was coincident with altered expression of EMT markers (Fig. 1A, 1B and 2A, S5B). Similarly, the appearance of BN and MN containing CDβgeo and SKBR3 cells also corresponded to changes in EMT markers (Fig. S1D, S1E and S3A). shRNA-mediated Smad4 depletion in MCF10A cells abrogated the increase in BN and MN cells and EMT (Fig. 2B and 2C).

To evaluate whether the mitotic errors specifically occur in mesenchymally transitioned cells, untreated and TGFβ-treated MCF10A cells were stained with E-Cadherin and Fibronectin (FN1), and percentages of BN and MN cells in each state were scored. Over 95% of untreated MCF10A cells were positive for only E-Cadherin (E+) and this fraction decreased to ~50% following 1 day of TGFβ treatment. Among these epithelial cells (E), the BN and MN fractions before and after TGFβ treatment ranged from 0.66±0.93% to

1.0±1.41% and 0.73±0.18% to 1.79%±0.29%, respectively (p=NS). Cells transitioning to the mesenchymal state (M) coexpressed both E-cadherin and FN1 (E+M+) or FN1 (M+) alone and increased from ~4% to ~50% before and after TGFβ treatment. Among these mesenchymal cells, BN (7.3±0.86%) and MN (5.54±64%) cell fractions were prevalent ($p<0.01$; Fig. 2D) suggesting that the mitotic defects induced by TGFβ occur primarily whithin mesenchymal cells. Furthermore, knockdown of ZEB1, a TGFβ-inducible transcriptional regulator of EMT (Miyazono, 2009), suppressed TGFβ-mediated EMT and decreased BN and MN cells compared with sh-Luciferase transfected TGFβ-treated controls (Fig. 2E and S3B).

To determine whether induction of mitotic defects is a general feature of EMT, we tested MCF10A cells expressing an inducible stable variant SNAIL-S6A and observed the simultaneous appearance of both EMT and mitotic aberrations (BN and MN containing cells) (Fig. 2F, and S3C). Similar results were observed in SKBR3 cells expressing inducible SNAIL (Fig. S3D and S3E). SNAIL expression significantly increased time for cell division (MCF10A cells, uninduced control: 58 ±46 min vs SNAIL-S6A induced: 100 ±106 min, $p<0.0001$; SKBR3 cells, uninduced control: 101 ±48 min vs SNAIL-S6A induced: 126 ±72 min, $p<0.001$; Fig. 2G and S3F).

Interestingly, MCF7, a predominantly epithelial breast cancer cell line that fails to undergo EMT in response to TGFβ, did not exhibit mitotic anomalies (Fig. S4A). Three cancer associated fibroblast (CAF) cell lines, derived from three different breast cancer patients neither undergo further mesenchymal changes nor exhibit mitotic defects following TGFβ treatment (Fig. S4B). Together, these findings raise the possibility that TGFβ-induced mitotic abnormalities in proliferating epithelial cells are linked to its ability to induce EMT in these cells.

Mitotic defects result from simultaneous proliferation of cells undergoing EMT

The incompatibility of EMT and cellular proliferation is supported by developmental failure of embryos lacking a timed mitotic block (Grosshans and Wieschaus, 2000; Mata et al., 2000; Murakami et al., 2004; Seher and Leptin, 2000). Normal epithelial cells treated with TGFβ arrest at the G1 phase of the cell cycle (Derynck et al., 2001; Massague, 2008). Indeed, freshly isolated normal mouse mammary epithelial cells (nMMECs) are highly sensitive to TGFβ-mediated growth inhibition and show no increase in mitotic anomalies despite the induction of EMT (Fig. 3A, 3B and 3C).

To expand upon this observation, we took advantage of the tight dependence of MCF10A cell proliferation on epidermal growth factor (EGF), and their growth arrest upon its withdrawal (Fig. 3D). TGFβ induces EMT without any mitotic defects in non-proliferative (EGF-depleted) MCF10A cells (Fig. 3E and S4C). Mitotic defects appear when EGF is added back in the presence of TGFβ (Fig. S4D). EMT and proliferation can be temporally separated in MCF10A cells, with transient addition of TGFβ to non-proliferating cells, followed by its withdrawal as EGF is added back to induce proliferation. Remarkably, MCF10A cells exposed to TGFβ while growth arrested fail to display mitotic defects when cell proliferation resumes in the absence of TGFβ (Fig. 3F). These results suggest that coincidence of cell proliferation during EMT compromises mitotic integrity.

Suppression of nuclear envelope (NE) proteins by EMT inducers

We quantitatively mapped the proteomes of untreated and TGFβ-treated MCF10A cells using multiplexed mass spectrometry (MS) (McAlister et al., 2014; Ting et al., 2011) to define the mechanisms underlying these mitotic aberrations. A total of 7191 unique proteins were quantified in TGFβ-treated cells (0, 1, and 6 days) in two independent replicate experiments (Fig. S5A, Concordance between replicates: Pearson correlation coefficient, r =0.70 between 0 vs 1 day TGFβ-treated samples; r =0.75 between 0 vs 6 day TGFβ-treated samples). The proteome differences between the 0 vs 1-day, and the 0 vs 6-day TGFβ-treated samples were well correlated (r =0.81) suggesting that the regulation of these proteins occurs as early as 24 hours after TGFβ treatment (Fig. 4A). TGFβ treatment decreased expression of several epithelial markers and increased many EMT-inducing transcription factors and mesenchymal markers (Fig. S5B). GSEA analysis of proteins induced by TGFβ identified 22 pathways involved in cytoskeletal organization (5 pathways), cell-cell and cell-matrix interactions (4 pathways), DNA damage responses (2 pathways) as well as chromosome-related biology (4 pathways) (all driven by ≥3 matching proteins; FDR≤0.25; Database 1, Fig. S5C and S5D). Similar analysis of proteins down-regulated by TGFβ (FDR≤0.05) identified 18 pathways involved in the architecture and function of mitochondria (11 pathways) and nucleus [(7 pathways) (Fig. 4B, 4C and Database 1)]. Specifically, several components of the NE [LMNB1 (laminB1), LBR (laminB receptor), NRM (nurim-nuclear envelope membrane protein), TMPO (the inner nuclear membrane protein Thymopoietin) and EMD (Emerin)], and multiple nucleoporins forming the nuclear pore complex (NUP54, NUP62, NUP88, NUP98, NUP 107, NUP133, NUP160, GLE1) were suppressed in proliferating cells undergoing EMT (Fig. 4B and 4C; Table S1, Database 1). MS analysis of SNAIL-inducible MCF10A cells also demonstrated that proteins involved in the mitochondrial and nuclear architecture and function (identified in TGFβ-treated samples) were significantly suppressed following SNAIL induction (Fig. 4D and S5E). Analysis of the RNASeq data of TGFβ- and SNAIL -induced MCF10A cells showed that suppression of the NE proteins by TGFβ and SNAIL was post-transcriptional, while the suppression of mitochondrial proteins occurred at the transcriptome level (Fig. 4E, S6A, S6B, S6C).

The suppression of NE proteins including Lamins in cells during TGFβ- and SNAIL-induced EMT was consistent with nuclear blebbing and circularity distortions (Funkhouser et al., 2013) observed in these cells (Fig. 5A, S7A, S7B). We then tested the NE integrity in TGFβ-treated MCF10A cells stably expressing YFP-fused to the nuclear localization signal (NLS) of SV40 large T antigen through real time imaging of the cells. Appearance of NLS-YFP in the cytoplasm with a concomitant decrease in nuclear signal in the absence of mitosis indicates nuclear envelope disruption (NED) in interphase cells, whereas reappearance of YFP nuclear signal is a measure of NE repair (Fig. 5B and S7C). NED during mitosis culminates in the appearance of two daughter nuclei [Fig. S7C(i)]. Real-time imaging of TGFβ-treated NLS-YFP-MCF10A cells showed increased NED at interphase [Untreated: 4.58×10^{-5}%, TGFβ 3 days: 79.3×10^{-5}%, TGFβ 8 days: 98.92×10^{-5}%; X^2 = 0.012; Fig. 5B and Fig. S7C(ii); Movie S4]. Time to repair NED in TGFβ-treated interphase cells ranged from 3.5 to 66.3 min (median of 12.23 min and mean± SE of 18.87 ± 5.01 min), compared to the time taken to reassemble the NE at the end of mitosis, which ranged from

26.2 to 42.7 minutes (median of 33.6 min and mean±SE of 34.04 ± 2.89 min, Fig. S7D). Together, these observations point to a profound defect in NE integrity during EMT, and are consistent with cell migration leading to NE disruption and repair (Denais et al., 2016; Raab et al., 2016).

To further validate the contribution of compromised NE integrity to the mitotic phenotypes induced by TGFβ, we selected LaminB1, a major determinant of nuclear shape and size with a dual role in regulating cytokinesis, spindle matrix and chromatin condensation (Gruenbaum and Foisner, 2015; Guttinger et al., 2009; Hayashi et al., 2016; Martin et al., 2010; Tsai et al., 2006; Verstraeten et al., 2011), for more detailed analysis. TGFβ suppressed Lamins A and B1 proteins in MCF10A, SKBR3 as well as CDβgeo cells, whereas its removal restored the levels of Lamins (Fig. 5C and S7E). The suppression of LaminB1 protein by TGFβ was independent of the proliferative status of the cells (Fig. S7F). SNAIL reduced LaminB1 but not LaminA protein in MCF10A and SKBR3 cells (Fig. S7G). The reduction in lamin proteins in TGFβ-treated cells, as evidenced by the RNASeq data, was not associated with changes in Lamin mRNA levels (Fig. S6B), or protein stability (Fig. 5D) suggesting that TGFβ-mediated suppression of Lamins might involve translational regulation.

We depleted LaminB1 in MCF10A cells to determine the functional consequence of decreased LaminB1 protein (Fig. 5E). Suppression of LaminB1 did not induce EMT but increased the number of BN (siControl: 0.59%±0.19% and siLaminB1: 2.41±0.32%), and MN cells (siControl: 1.15%±0.15% and siLaminB1: 2.43±0.26%; $p<0.01$, Fig. 5E). We then tested whether expression of ectopic laminB1 would reverse the mitotic defects in TGFβ-treated cells. Expression of ectopic laminB1 protein was two-fold higher compared to endogenous levels (Fig. 5F) but declined following TGFβ exposure (consistent with TGFβ-mediated translational regulation of LaminB1), yet it remained 2-fold higher compared to the TGFβ-treated vector controls and did not affect TGFβ-induced EMT markers (Fig. 5F). Ectopic expression of LaminB1 significantly reduced TGFβ-mediated appearance of BN (Vector-untreated: 1.28%±0.21%; Vector-TGFβ-treated: 11.44%±0.39%; LaminB1-untreated: 2.32%±0.39%; LaminB1-TGFβ-treated: 5.48%±1.17%), and MN cells (Vector-untreated: 1.13%±0.21%; Vector-TGFβ-treated: 9.55%±1.05%; LaminB1-untreated: 1.22% ±0.31%; LaminB1-TGFβ-treated: 5.54%±0.87%; $p<0.01$; Fig. 5F). Moreover, restoring LaminB1 protein reduced the number of mitotic events with cytokinesis failure (Vector-TGFβ-treated: 7%; LaminB1-TGFβ-treated:1%), and decreased the duration of cell division in TGFβ-treated cultures (Fig. 5G).

EMT promotes genomic instability and tumorigenicity

We quantified the heritable genetic abnormalities induced by TGFβ using interphase FISH against four representative chromosomes: 2, 4, 17 and 21. MCF10A cells treated with TGFβ for 12 days were allowed to revert to an epithelial state (mesenchymal to epithelial transition – MET) and reach equilibrium (for 12 days after cytokine withdrawal) to measure stably heritable changes (Fig. 6A and S8A). At baseline, 96–98% of MCF10A cells are diploid for each of the 4 chromosomes. TGFβ induced a significant loss of chromosome 2 ($X^2 = 0.024$), and gain in chromosomes 2 ($X^2 = 0.002$), 4 ($X^2 = 0.0256$), and 21 ($X^2 = 0.00076$) compared

to untreated controls (Fig. 6A). Of note, 3/454 TGFβ-exposed cells had gained 4 copies of all four chromosomes, suggesting the emergence of a minor population of polyploid cells [(0.66%) (Fig. S8A)]. This is consistent with polyploidy being a problem for the normal completion of mitosis, resulting in loss of chromosomes and aneuploidy (Comai, 2005). The gain of chromosomes in cells with a history of TGFβ exposure was highly significant (X^2=0.0002). MCF10A cells with a history of EMT induction through ectopic expression of SNAIL for 9 days also exhibited the emergence of polyploid cells (0.97%; p=0.001; Fig. S8B).

Sustained aneuploidy was also observed in CDβgeo cells (n=78), which exhibit chromosome number variation at baseline, with subpopulations that are diploid (30.7%), hypodiploid (14%) and aneuploid (3.8% between 4N-6N, and 2.6% >6N) (Fig. 6B and S8C). TGFβ (n=57) increased aneuploidy with 35% of cells showing massive polyploidy (15.8% with 4N-6N, and 19.3% with 6N-24N; $X^2=6\times10^{-5}$; Fig. 6B and S8C). Following TGFβ withdrawal, a newly derived genetically diverse subpopulation of cells with ~5N chromosomes emerged (32.5% of cells with 4N-6N, 1.7% of cells with 6N-24N; $X^2=6\times10^{-5}$; Fig. 6B and S8C). This effect is distinct from that of general oncogenic drivers, since no significant change in ploidy was observed with oncogenic HRAS, which triggers tumorigenicity but not EMT in CDβgeo cells (Fig. 6B and S8D). Thus, the effect of TGFβ exposure on ploidy is distinct from any general proliferative or oncogenic effect, but is dependent on EMT.

We then tested whether TGFβ-induced chromosomal abnormalities contribute to tumorigenic phenotypes. CDβgeo cells, which exhibit genomic instability following exposure to TGFβ (Fig. 6B), are more metastatic in mice (Fig. S8E). Exposure of proliferating MCF10A cells to TGFβ promoted their growth in soft agar, a characteristic *in vitro* correlate of tumorigenic potential (p=0.02, Fig. 6C). Interestingly, non-proliferating MCF10A cells (grown without EGF) treated with TGFβ, which do not exhibit genomic instability (Fig 3D, 3E), were not able to grow in soft agar (Fig. 6C).

In contrast to untreated MCF10A cells and non-proliferating MCF10A cells treated with TGFβ, 3 out of 5 selected soft agar colonies derived from proliferating MCF10A cells exposed to TGFβ were tumorigenic in mice (Fig. S8F). Remarkably, 2D-culture of these tumor-derived cells showed a high degree of genomic heterogeneity, with a mean of ~3N chromosomal content (Fig. 6D). Taken together these results show that exposure of proliferating cells to TGFβ triggers tumorigenic properties, with the resulting tumors being enriched for a genomically diverse and heterogeneous cell populations.

Mesenchymal CTCs from metastatic breast cancer patients exhibit genomic instability

We recently demonstrated changes in EMT expression patterns in circulating tumor cells (CTCs) isolated from the blood of women with metastatic breast cancer. CTCs stained by RNA-ISH using multiple probes that mark the epithelial (CDH1, EPCAM, KRT5, 7, 8, 18, 19) and mesenchymal (FN1, CDH2, SERPINE1 (PAI1) states identified the CTCs to be present in either epithelial (E) or mesenchymal (M) states (Yu et al., 2013). We assessed these epithelial and mesenchymal CTC populations for the presence of MN, a proxy of genomic instability. Evaluation of 238 CTCs (E>M in 109 CTCs and M>E in 129 CTCs)

isolated from 11 individual blood draws showed the presence of MN in ~3.9% of mesenchymal CTCs and none (0%) in the epithelial CTCs (p=0.036, Fig. 7A). Given the limited number of patients in our analysis, we do not exclude the possibility that MN are present in epithelial CTCs at a low frequency. Moreover, 10.8% of the mesenchymal CTCs were binucleated compared to 1.8% of epithelial CTCs (p=0.004, Fig. 7A). These data, consistent with our in vitro findings shown in Fig. 2D, suggest that EMT is one of a variety of mechanisms promoting MN formation.

We also interrogated whether EMT and TGFβ associated signatures in CTCs are correlated with aneuploidy. We analyzed nine TGFβ, nine EMT and six aneuploidy metagene signatures (Table S2) in RNASeq data derived from pure populations of CTCs isolated from the blood of women with metastatic breast cancer (Aceto et al., 2014), and from single CTCs isolated from men with metastatic prostate cancer (Miyamoto et al., 2015). A positive Pearson correlation between TGFβ, EMT and aneuploidy signatures, ranging from 0.4–1.0 (FDR<0.1) in the breast CTCs and in the prostate CTCs (FDR<0.1), was observed (Fig. 7B, 7C). Compared with these purified populations of metastatic breast and prostate cancer cells, primary tumor TCGA data showed weaker correlations, consistent with the smaller fraction of cells within primary tumors exhibiting EMT [(Yu et al., 2013) (Fig. 7B and 7C)].

Discussion

Whereas normal cells cease proliferation during developmentally programmed EMT (Grosshans and Wieschaus, 2000; Mata et al., 2000; Murakami et al., 2004; Seher and Leptin, 2000), we show that epithelial cancer cells failing to arrest during EMT (Derynck et al., 2001; Massague, 2008) exhibit mitotic errors and genomic instability. While EMT itself is reversible upon TGFβ and SNAIL withdrawal, the induced abnormalities in ploidy and genomic heterogeneity are heritable. The clinical significance of these findings is supported by the prevalence of mitotic abnormalities, binucleation and MN, in single CTCs of mesenchymal lineage in metastatic breast cancer patients.

TGFβ induces BN cells with extra centrosomes leading to multipolar spindle attachments. However, multipolar anaphase, known to result in inviable progeny (Ganem et al., 2009), was never observed. Instead, TGFβ-treated mitotic cells undergo centrosome clustering and bipolar division causing chromosome missegregation and increased duration of mitosis. Cytokinesis failure and MN formation cause extensive damage to missegregating chromosomes (Crasta et al., 2012; Janssen et al., 2011). In fact, TGFβ increases DNA damage in cells (Fig. S2E), which in turn propagates additional missegregation events (Bakhoum et al., 2014; Burrell et al., 2013) exacerbating genomic instability in cells undergoing EMT. This ultimately leads to heritable changes in the genomic composition of these cells.

Mass Spectrometric analysis of proteins indicates that the NE integrity is severely compromised in cells undergoing EMT. Migrating cells experience strong physical forces that deform the nucleus, whose mechanical stability is maintained by the NE (Gruenbaum and Foisner, 2015). Suppression of NE proteins including LaminB1 by TGFβ and SNAIL is likely to weaken the NE, compromising its ability to withstand the mechanical stress exerted

on the nucleus during EMT. This deformation of nuclear structure causes nucleoplasm leakage into the cytoplasm during interphase. In fact, cell migration is shown to result in NE rupture and the loss of nuclear and cytoplamic compartmentalization (Denais et al., 2016; Raab et al., 2016). NE collapse results in mislocalization of cytoplasmic and nuclear proteins, and the entrapment of cytoplasmic organelles in the nucleus (Vargas et al., 2012). Exposure of DNA to the deleterious effects of the cytoplasm triggers extensive DNA damage and fragmentation, and ultimately chromothripsis (Crasta et al., 2012; Hatch et al., 2013). Thus, a deformed NE and NED at interphase during EMT could have profound consequences on genomic integrity, and may help drive the mutational instability of these cells.

Many components of the NE and nuclear pore complexes are crucial to orchestrating proper mitotic progression (Gruenbaum and Foisner, 2015; Guttinger et al., 2009). TGFβ- and SNAIL suppress multiple NE and nuclear pore components, which are critical for mitosis, spindle activation checkpoint and assembly and maintenance of NE function (Gruenbaum and Foisner, 2015; Guttinger et al., 2009). Suppression of these proteins is likely to be responsible for the mitotic defects in proliferating cells undergoing EMT. Specifically, LaminB1, suppressed by TGFβ and SNAIL, plays an important role in cytokinesis, spindle assembly and chromatin condensation (Funkhouser et al., 2013; Hayashi et al., 2016; Martin et al., 2010; Tsai et al., 2006; Verstraeten et al., 2011). Disruption of LaminB1 causes cause nuclear blebbing (Funkhouser et al., 2013), and cytokinesis failure leading to BN and MN cells (Funkhouser et al., 2013; Hayashi et al., 2016; Martin et al., 2010; Tsai et al., 2006; Verstraeten et al., 2011), thus, phenocopying the effects of TGFβ. Accordingly, restoring LaminB1 partially rescues the mitotic abnormalities induced by TGFβ suggesting that additional NE components suppressed by TGFβ are also likely to contribute to the cytokinesis and mitotic defects observed in cells undergoing EMT.

Mitotic defects constitute an important mechanism that promotes cancer progression and genomic instability. Gene copy number changes may affect the levels of critical regulators of cellular homeostasis, while chromosome losses may induce homozygosity for point mutations in tumor suppressors, and chromosome translocations may directly disrupt critical genes. Chromothripsis was identified as a unique mechanism of chromosomal shredding that occurs in some cancers (Lee et al., 2016). While single cell whole genome sequencing would be required to assess whether TGFβ-treatment induces chromothripsis, the extent of micronucleation observed in these cultures suggests that it may set the stage for accelerated cancer progression, together with aneuploidy and polyploidy resulting from chromosomal nondisjunction and disrupted mitotic spindles. Of note, the gross aneuploidy observed in TGFβ-treated cultures appears to reach a new stable equilibrium with increased ploidy of ~3N (Fig. 6D). Cells establishing aneuploidy following genomic doubling and eventual chromosome loss have been described as a means of faster adaption and fitness gain (Chen et al., 2012; Dewhurst et al., 2014; Selmecki et al., 2015). In fact, the average estimated ploidy in a wide range of human tumors was shown to be close to 3.3N (Zack et al., 2013), suggesting that triploid karyotypes frequently emerge from tetraploid cells exhibiting reduction in ploidy over time (Carter et al., 2012; Dewhurst et al., 2014). Together, these observations provide a mechanistic explanation for the reported link between TGFβ expression in stromal fibroblasts and tumor aggressiveness (Nguyen et al., 2011).

Our observations also highlight a powerful role for tumor-stromal interactions: Stroma-derived paracrine growth-inducing and survival signals besides sustaining adjacent cancer cells, may also induce heritable genetic defects within cancer cells and increase genomic variation. In seminal experiments, Weinberg and colleagues demonstrated that cancer-associated fibroblasts can enhance tumorigenicity of associated cancer cells over many generations (Orimo et al., 2005). Our results are consistent with this model and provide a potential mechanism to explain these observations. To date, the pleiotropic nature of TGFβ signaling has prevented the therapeutic targeting of this pathway, which may either enhance or suppress tumorigenesis depending on cellular context. The possibility that TGFβ may enhance genomic instability early in tumorigenesis raises the possibility that TGFβ inhibition may have a role in cancer preventive strategies.

Methods

Cell Culture, siRNA transfection and Lentiviral expression

The culture of MCF10A, CDβgeo and SKBR3 cells, as well as the derivation and culture of normal mouse mammary epithelial cells, human cancer associated fibroblasts (CAFs), stable H2B–RFP expressing MCF10A and SKBR3 cell lines and stable YFP-NLS expressing MCF10A cell lines are described in the supplementary methods. Stable expression of LaminB1 was performed by stable lentiviral transfection of pLenti-LaminB1. siRNA against LaminB1 (#1 s8226, #2 s8225, Ambion) and siControl (silencer negative control #1, Ambion) were transfected at 10 nM concentration into cells. Detailed protocols are provided in the supplementary methods.

Western blot

The antibodies used were against E-Cadherin (BD 610181), PAI1 (BD 612024), Fibronectin (Sigma-Aldrich), Vimentin (BD 550513), Smad4 (Cell Signaling Technology), CK8 (Abcam), SNAIL (Cell Signaling Technology), LaminA/C (Abcam), LaminA (Sigma), LaminB1 (Abcam) GAPDH (Millipore ABS16), and IRDye-800 anti-Rabbit (Rockland), or IRDye-680 anti-mouse (Rockland), and HRP-conjugated anti-mouse or anti-rabbit (Jackson laboratory) antibodies.

In vivo tumorigenesis assay

All mice were cared for and experiments were performed under AALAS guidelines using protocols approved by the institutional review board and the institutional animal care and use committee of the Massachusetts General Hospital.

Immunostaining and Cytogenetic analysis of chromosome spreads

Immunostaining and cytogenetic analysis of cells were performed as described in supplementary methods.

Cell preparation and FISH analysis

Fluorescence in situ hybridization (FISH) performed using four locus-specific probes mapping to four different autosomes as well as data analysis of interphase cells are described in supplementary methods.

Quantitative Proteomics

Sample preparation, analysis on the mass spectrometer and functional analysis of quantitative proteomics are described in the supplementary methods.

Bioinformatic analysis

Bioinformatic analysis to determine the correlation between TGFβ, EMT, and Aneuploidy signatures in human breast and prostate cancer samples is described in supplementary methods.

Additional experimental protocols are provided in detail in supplementary methods.

Supplementary Material

Refer to Web version on PubMed Central for supplementary material.

Acknowledgments

Grant Support

This work was supported by grants from the Susan G. Komen for the Cure KG09042 (S.M.), ESSCO-MGH Breast Cancer Research Fund (S.M.), NCI Federal Share Program and Income (S.M.), Philippe Foundation Grant (V.C, R.B), Stand Up to Cancer (D.A. H., S. M), Breast Cancer Research Foundation (D.A.H.), National Foundation for Cancer Research (D.A.H.), Howard Hughes Medical Institute (D.A.H.), NIH CA129933 (D.A.H.), NIH GM076388 (L.Z.). L.Z. is a Jim & Ann Orr MGH Research Scholar. S.R. is a Samana Cay MGH Research Scholar. N.A. is a fellow of the Human Frontiers Science Program, the Swiss National Science Foundation, and the Swiss Foundation for Grants in Biology and Medicine. R.B. is supported by the Tosteson Postdoctoral Fellowship Award and the Marsha Rivkin Scientific Scholar Award.

We would like to thank Drs. Joseph Jerry and Karen Dunphy (University of Massachusetts, Amherst, MA 01003) for the CDβgeo cells, Dr. Linda Nieman and Tiffany N. Lewis (MGH Cancer Center) for helping with time-lapse imaging of cells, Drs. Cristina Montagna and Jidong Shan (Albert Einstein College of Medicine, NY) for interphase DNA-FISH analysis, Dr. Nick Dyson for critical reading of the manuscript, and Ms. Laura Libby and Mr. Daniel Garcia Garcia for technical support.

References

Aceto N, Bardia A, Miyamoto DT, Donaldson MC, Wittner BS, Spencer JA, Yu M, Pely A, Engstrom A, Zhu H, et al. Circulating tumor cell clusters are oligoclonal precursors of breast cancer metastasis. Cell. 2014; 158:1110–1122. [PubMed: 25171411]

Bakhoum SF, Kabeche L, Murnane JP, Zaki BI, Compton DA. DNA-damage response during mitosis induces whole-chromosome missegregation. Cancer Discov. 2014; 4:1281–1289. [PubMed: 25107667]

Burrell RA, McGranahan N, Bartek J, Swanton C. The causes and consequences of genetic heterogeneity in cancer evolution. Nature. 2013; 501:338–345. [PubMed: 24048066]

Carter SL, Cibulskis K, Helman E, McKenna A, Shen H, Zack T, Laird PW, Onofrio RC, Winckler W, Weir BA, et al. Absolute quantification of somatic DNA alterations in human cancer. Nat Biotechnol. 2012; 30:413–421. [PubMed: 22544022]

Chen G, Bradford WD, Seidel CW, Li R. Hsp90 stress potentiates rapid cellular adaptation through induction of aneuploidy. Nature. 2012; 482:246–250. [PubMed: 22286062]

Comai L. The advantages and disadvantages of being polyploid. Nat Rev Genet. 2005; 6:836–846. [PubMed: 16304599]

Crasta K, Ganem NJ, Dagher R, Lantermann AB, Ivanova EV, Pan Y, Nezi L, Protopopov A, Chowdhury D, Pellman D. DNA breaks and chromosome pulverization from errors in mitosis. Nature. 2012; 482:53–58. [PubMed: 22258507]

Denais CM, Gilbert RM, Isermann P, McGregor AL, Te Lindert M, Weigelin B, Davidson PM, Friedl P, Wolf K, Lammerding J. Nuclear envelope rupture and repair during cancer cell migration. Science. 2016

Derynck R, Akhurst RJ, Balmain A. TGF-beta signaling in tumor suppression and cancer progression. Nat Genet. 2001; 29:117–129. [PubMed: 11586292]

Dewhurst SM, McGranahan N, Burrell RA, Rowan AJ, Gronroos E, Endesfelder D, Joshi T, Mouradov D, Gibbs P, Ward RL, et al. Tolerance of whole-genome doubling propagates chromosomal instability and accelerates cancer genome evolution. Cancer Discov. 2014; 4:175–185. [PubMed: 24436049]

Fischer KR, Durrans A, Lee S, Sheng J, Li F, Wong ST, Choi H, El Rayes T, Ryu S, Troeger J, et al. Epithelial-to-mesenchymal transition is not required for lung metastasis but contributes to chemoresistance. Nature. 2015; 527:472–476. [PubMed: 26560033]

Funkhouser CM, Sknepnek R, Shimi T, Goldman AE, Goldman RD, Olvera de la Cruz M. Mechanical model of blebbing in nuclear lamin meshworks. Proc Natl Acad Sci U S A. 2013; 110:3248–3253. [PubMed: 23401537]

Ganem NJ, Godinho SA, Pellman D. A mechanism linking extra centrosomes to chromosomal instability. Nature. 2009; 460:278–282. [PubMed: 19506557]

Grosshans J, Wieschaus E. A genetic link between morphogenesis and cell division during formation of the ventral furrow in Drosophila. Cell. 2000; 101:523–531. [PubMed: 10850494]

Gruenbaum Y, Foisner R. Lamins: nuclear intermediate filament proteins with fundamental functions in nuclear mechanics and genome regulation. Annu Rev Biochem. 2015; 84:131–164. [PubMed: 25747401]

Guttinger S, Laurell E, Kutay U. Orchestrating nuclear envelope disassembly and reassembly during mitosis. Nat Rev Mol Cell Biol. 2009; 10:178–191. [PubMed: 19234477]

Hatch EM, Fischer AH, Deerinck TJ, Hetzer MW. Catastrophic nuclear envelope collapse in cancer cell micronuclei. Cell. 2013; 154:47–60. [PubMed: 23827674]

Hayashi D, Tanabe K, Katsube H, Inoue YH. B-type nuclear lamin and the nuclear pore complex Nup107–160 influences maintenance of the spindle envelope required for cytokinesis in Drosophila male meiosis. Biol Open. 2016

Janssen A, van der Burg M, Szuhai K, Kops GJ, Medema RH. Chromosome segregation errors as a cause of DNA damage and structural chromosome aberrations. Science. 2011; 333:1895–1898. [PubMed: 21960636]

Kim ES, Kim MS, Moon A. TGF-beta-induced upregulation of MMP-2 and MMP-9 depends on p38 MAPK, but not ERK signaling in MCF10A human breast epithelial cells. Int J Oncol. 2004; 25:1375–1382. [PubMed: 15492828]

Labelle M, Begum S, Hynes RO. Direct signaling between platelets and cancer cells induces an epithelial-mesenchymal-like transition and promotes metastasis. Cancer Cell. 2011; 20:576–590. [PubMed: 22094253]

Lee JK, Choi YL, Kwon M, Park PJ. Mechanisms Consequences of Cancer Genome Instability: Lessons from Genome Sequencing Studies. Annu Rev Pathol. 2016

Maheswaran S, Haber DA. Cell fate: Transition loses its invasive edge. Nature. 2015; 527:452–453. [PubMed: 26560026]

Martin C, Chen S, Jackson DA. Inheriting nuclear organization: can nuclear lamins impart spatial memory during post-mitotic nuclear assembly? Chromosome Res. 2010; 18:525–541. [PubMed: 20568006]

Massague J. TGFbeta in Cancer. Cell. 2008; 134:215–230. [PubMed: 18662538]

Mata J, Curado S, Ephrussi A, Rorth P. Tribbles coordinates mitosis and morphogenesis in Drosophila by regulating string/CDC25 proteolysis. Cell. 2000; 101:511–522. [PubMed: 10850493]

McAlister GC, Nusinow DP, Jedrychowski MP, Wuhr M, Huttlin EL, Erickson BK, Rad R, Haas W, Gygi SP. MultiNotch MS3 enables accurate, sensitive, and multiplexed detection of differential expression across cancer cell line proteomes. Anal Chem. 2014; 86:7150–7158. [PubMed: 24927332]

Miyamoto DT, Zheng Y, Wittner BS, Lee RJ, Zhu H, Broderick KT, Desai R, Fox DB, Brannigan BW, Trautwein J, et al. RNA-Seq of single prostate CTCs implicates noncanonical Wnt signaling in antiandrogen resistance. Science. 2015; 349:1351–1356. [PubMed: 26383955]

Miyazono K. Transforming growth factor-beta signaling in epithelial-mesenchymal transition and progression of cancer. Proc Jpn Acad Ser B Phys Biol Sci. 2009; 85:314–323.

Murakami MS, Moody SA, Daar IO, Morrison DK. Morphogenesis during Xenopus gastrulation requires Wee1-mediated inhibition of cell proliferation. Development. 2004; 131:571–580. [PubMed: 14711880]

Nguyen DH, Oketch-Rabah HA, Illa-Bochaca I, Geyer FC, Reis-Filho JS, Mao JH, Ravani SA, Zavadil J, Borowsky AD, Jerry DJ, et al. Radiation acts on the microenvironment to affect breast carcinogenesis by distinct mechanisms that decrease cancer latency and affect tumor type. Cancer Cell. 2011; 19:640–651. [PubMed: 21575864]

Nieto MA, Huang RY, Jackson RA, Thiery JP. Emt: 2016. Cell. 2016; 166:21–45. [PubMed: 27368099]

Ocana OH, Corcoles R, Fabra A, Moreno-Bueno G, Acloque H, Vega S, Barrallo-Gimeno A, Cano A, Nieto MA. Metastatic colonization requires the repression of the epithelial-mesenchymal transition inducer Prrx1. Cancer Cell. 2012; 22:709–724. [PubMed: 23201163]

Olive PL, Banath JP. The comet assay: a method to measure DNA damage in individual cells. Nat Protoc. 2006; 1:23–29. [PubMed: 17406208]

Orimo A, Gupta PB, Sgroi DC, Arenzana-Seisdedos F, Delaunay T, Naeem R, Carey VJ, Richardson AL, Weinberg RA. Stromal fibroblasts present in invasive human breast carcinomas promote tumor growth and angiogenesis through elevated SDF-1/CXCL12 secretion. Cell. 2005; 121:335–348. [PubMed: 15882617]

Puisieux A, Brabletz T, Caramel J. Oncogenic roles of EMT-inducing transcription factors. Nat Cell Biol. 2014; 16:488–494. [PubMed: 24875735]

Raab M, Gentili M, de Belly H, Thiam HR, Vargas P, Jimenez AJ, Lautenschlaeger F, Voituriez R, Lennon-Dumenil AM, Manel N, Piel M. ESCRT III repairs nuclear envelope ruptures during cell migration to limit DNA damage and cell death. Science. 2016

Seher TC, Leptin M. Tribbles, a cell-cycle brake that coordinates proliferation and morphogenesis during Drosophila gastrulation. Curr Biol. 2000; 10:623–629. [PubMed: 10837248]

Selmecki AM, Maruvka YE, Richmond PA, Guillet M, Shoresh N, Sorenson AL, De S, Kishony R, Michor F, Dowell R, Pellman D. Polyploidy can drive rapid adaptation in yeast. Nature. 2015; 519:349–352. [PubMed: 25731168]

Soule HD, Maloney TM, Wolman SR, Peterson WD Jr, Brenz R, McGrath CM, Russo J, Pauley RJ, Jones RF, Brooks SC. Isolation and characterization of a spontaneously immortalized human breast epithelial cell line, MCF-10. Cancer Res. 1990; 50:6075–6086. [PubMed: 1975513]

Tam WL, Weinberg RA. The epigenetics of epithelial-mesenchymal plasticity in cancer. Nat Med. 2013; 19:1438–1449. [PubMed: 24202396]

Thiery JP, Lim CT. Tumor dissemination: an EMT affair. Cancer Cell. 2013; 23:272–273. [PubMed: 23518345]

Ting L, Rad R, Gygi SP, Haas W. MS3 eliminates ratio distortion in isobaric multiplexed quantitative proteomics. Nat Methods. 2011; 8:937–940. [PubMed: 21963607]

Tsai MY, Wang S, Heidinger JM, Shumaker DK, Adam SA, Goldman RD, Zheng Y. A mitotic lamin B matrix induced by RanGTP required for spindle assembly. Science. 2006; 311:1887–1893. [PubMed: 16543417]

Vargas JD, Hatch EM, Anderson DJ, Hetzer MW. Transient nuclear envelope rupturing during interphase in human cancer cells. Nucleus. 2012; 3:88–100. [PubMed: 22567193]

Verstraeten VL, Peckham LA, Olive M, Capell BC, Collins FS, Nabel EG, Young SG, Fong LG, Lammerding J. Protein farnesylation inhibitors cause donut-shaped cell nuclei attributable to a centrosome separation defect. Proc Natl Acad Sci U S A. 2011; 108:4997–5002. [PubMed: 21383178]

Ye X, Tam WL, Shibue T, Kaygusuz Y, Reinhardt F, Ng Eaton E, Weinberg RA. Distinct EMT programs control normal mammary stem cells and tumour-initiating cells. Nature. 2015; 525:256–260. [PubMed: 26331542]

Yu M, Bardia A, Wittner BS, Stott SL, Smas ME, Ting DT, Isakoff SJ, Ciciliano JC, Wells MN, Shah AM, et al. Circulating breast tumor cells exhibit dynamic changes in epithelial and mesenchymal composition. Science. 2013; 339:580–584. [PubMed: 23372014]

Zack TI, Schumacher SE, Carter SL, Cherniack AD, Saksena G, Tabak B, Lawrence MS, Zhsng CZ, Wala J, Mermel CH, et al. Pan-cancer patterns of somatic copy number alteration. Nat Genet. 2013; 45:1134–1140. [PubMed: 24071852]

Zheng X, Carstens JL, Kim J, Scheible M, Kaye J, Sugimoto H, Wu CC, LeBleu VS, Kalluri R. Epithelial-to-mesenchymal transition is dispensable for metastasis but induces chemoresistance in pancreatic cancer. Nature. 2015; 527:525–530. [PubMed: 26560028]

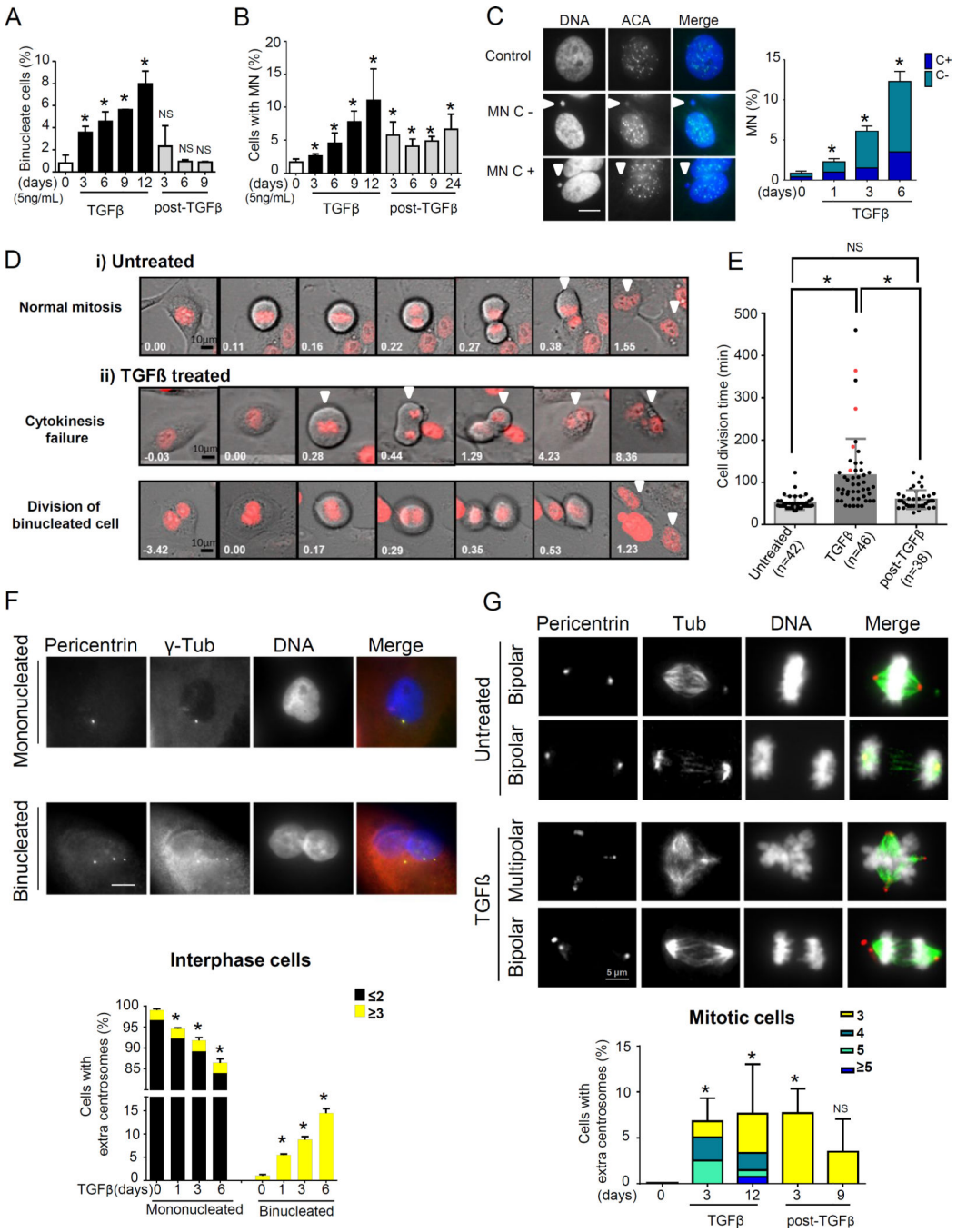

Figure 1. TGFβ-induces mitotic abnormalities

A) Percentages of BN and B) MN harboring in MCF10A cells following TGFβ treatment and its withdrawal. Cells were quantified after phalloidin and DAPI staining. Data represent mean ± s.d. derived from three independent experiments; *p<0.05, NS: not significant.

C) Representative images (left) and percentages of centromere-positive (MN C+) and –negative (MN C-) micronuclei (right; arrowheads) in TGFβ-treated MCF10A cells stained with an anti-centromere antibody (ACA) and DAPI. Data represent mean ± s.d. derived from

two independent experiments (*p<0.05; n≥1000 cells per condition). Scale bars represent 10μ.

D) Cytokinesis failure in TGFβ-treated cells results in BN cells.
Photomicrographs of live-imaged RFP-tagged H2B expressing MCF10A cells undergoing mitosis: (i) Untreated control; arrowheads show daughter cells, (ii) Upper: Cells treated with TGFβ for 12 days showing cytokinesis failure (arrowheads) resulting in a BN cell containing MN; (ii) Lower: shows the division of a binucleate cell. Arrowheads show daughter nuclei. Time is shown in hr:min. Scale bars represent 10μ.

E) Cell division time of RFP-tagged H2B expressing MCF10A cells [untreated, TGFβ-treated, and following TGFβ withdrawal after 9 days of exposure (post-TGFβ)]. Red dots denote BN cells with cytokinesis failure. *p<0.0001.

F) Cytokinesis failure of TGFβ-treated cells results in BN cells with extra centrosomes. Cells were stained for pericentrin, γ-tubulin and DAPI to mark the centrosomes, microtubules, and nuclei respectively. Images show 1 and 3 centrosomes in mono- and bi-nucleated interphase cells, respectively. Nuclei in the BN cells are not connected through a midbody. Graph shows the percentages of mono- and bi-nucleated cells in untreated and in TGFβ treated interphase MCF10A cells and the fraction of cells harboring ≤2 (black) and ≥3 (yellow) centrosomes in each population. Data represent mean ± s.d. derived from two independent experiments (*p<0.05, mononucleated ≥1000 cells, binucleated ≥ 185 cells). Scale bars represent 10μ.

G) Defective mitosis in TGFβ–treated cells. Pericentrin, tubulin and DAPI staining of untreated and TGFβ -treated cells. Upper: Normal bipolar mitotic events in untreated control cells. Lower: Multipolar spindle attachment and bipolar anaphase with centrosome clustering in TGFβ-treated cells. Graph shows the percentage of mitotic cells with extra centrosomes, and the fraction of cells harboring 3, 4, 5, and ≥5 centrosomes in untreated, TGFβ-treated and post-TGFβ MCF10A cell cultures. (n=3 independent experiments). The total number of events evaluated for each category: Untreated - 172; TGFβ (3days) - 134; TGFβ (12 days) - 204; post-TGFβ (3 days) - 87; post-TGFβ (9 days) - 93.

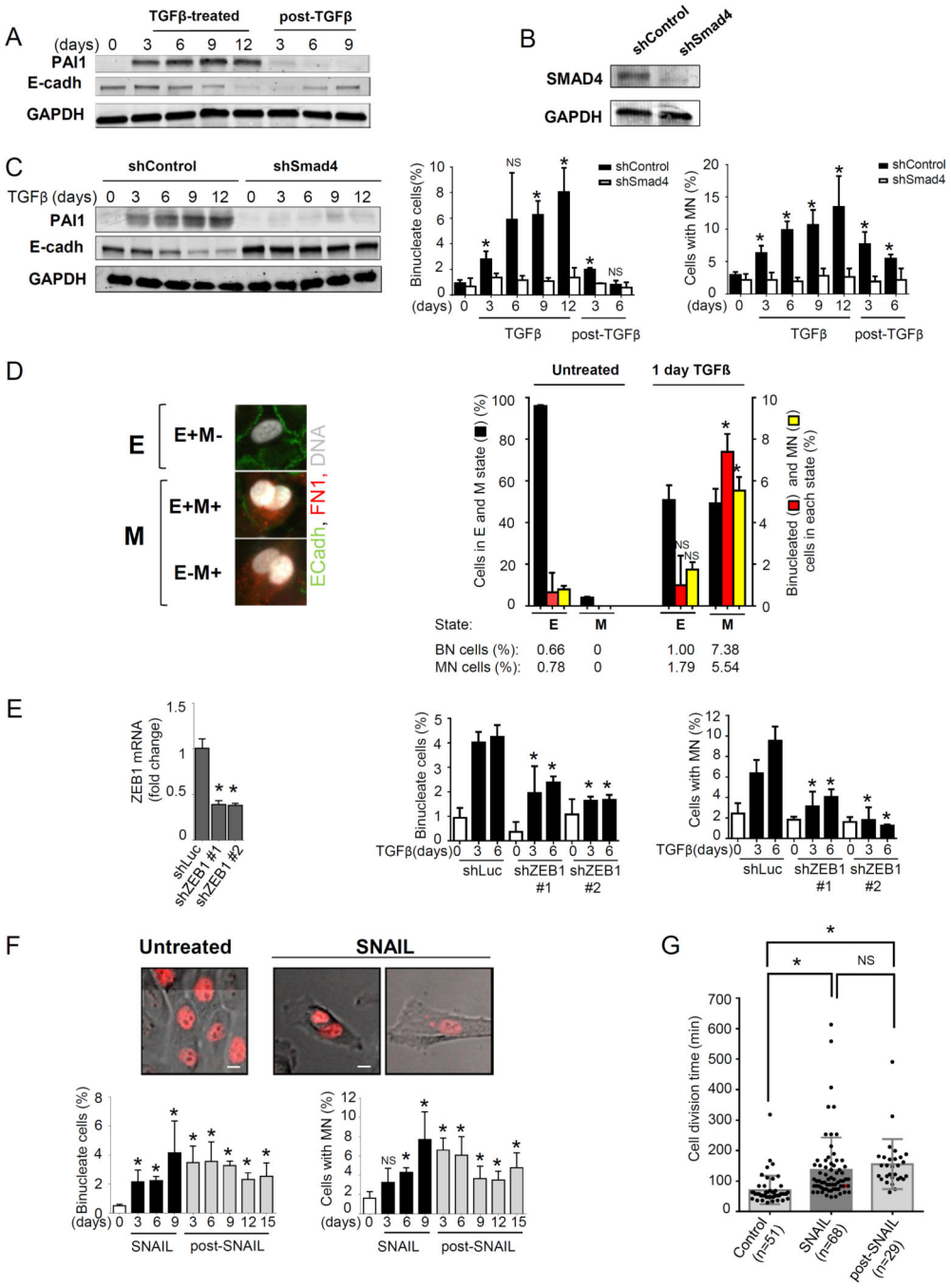

Figure 2. TGFβ-induced mitotic aberrations are dependent on EMT

A) Expression of mesenchymal marker, PAI1, and epithelial marker, E-Cadherin, in MCF10A cells following TGFβ treatment, and its withdrawal.

B) Expression of Smad4 protein in MCF10A cells infected with shControl or shSmad4.

C) (Left) PAI1 and E-Cadherin expression in TGFβ-treated shControl- and Smad4-depleted cells. (Right) Graphs show the percentages of BN and MN cells in TGFβ-treated shControl- and shSmad4 MCF10A cultures and following its withdrawal (post-TGFβ) [shControl

(*p<0.005); shSmad4 (NS: not significant)]. Data represent mean ± s.d. derived from three independent experiments.

D) TGFβ-induced mitotic aberrations are prevalent in mesenchymal cells. Untreated and TGFβ-treated cells were stained for E-cadherin, Fibronectin and with DAPI. Left: Images of cells expressing E-cadherin (epithelial-E+) alone, or transitioning to a mesenchymal state and expressing E-cadherin and Fibronectin (E+M+) or fibronectin (M+) alone. Graph shows the percentage of cells in the E (E+) and M (E+M+, and M+) states (black). Red and yellow bars represent the percentages of BN and MN cells within each state, respectively. Data represent mean ± s.d. derived from 3 independent fields from two independent experiments (*p<0.05). Scale bars represent 10μ.

E) ZEB1 depletion mitigates TGFβ-induced EMT. Left: ZEB1 knockdown in MCF10A cells. Quantification of BN and MN harboring cells in untreated and TGFβ-treated shLuc and shZEB1-MCF10A cultures. * p<0.001.

F) SNAIL induces BN and MN cells in RFP-tagged H2B expressing MCF10A cells. Non-induced cells are shown as control. Scale bars represent 10μ. Lower: Quantification of BN and MN harboring cells in control and SNAIL induced cultures. Data represent are mean ± s.d. derived from three independent experiments, *p<0.05; NS: not significant.

G) Cell division time of RFP-tagged H2B expressing MCF10A cells following 9 days of SNAIL induction (SNAIL), and its withdrawal for 15 days (post-SNAIL). Non-induced cells are shown as control. The number of cells analyzed for each condition is provided. *p<0.0001.

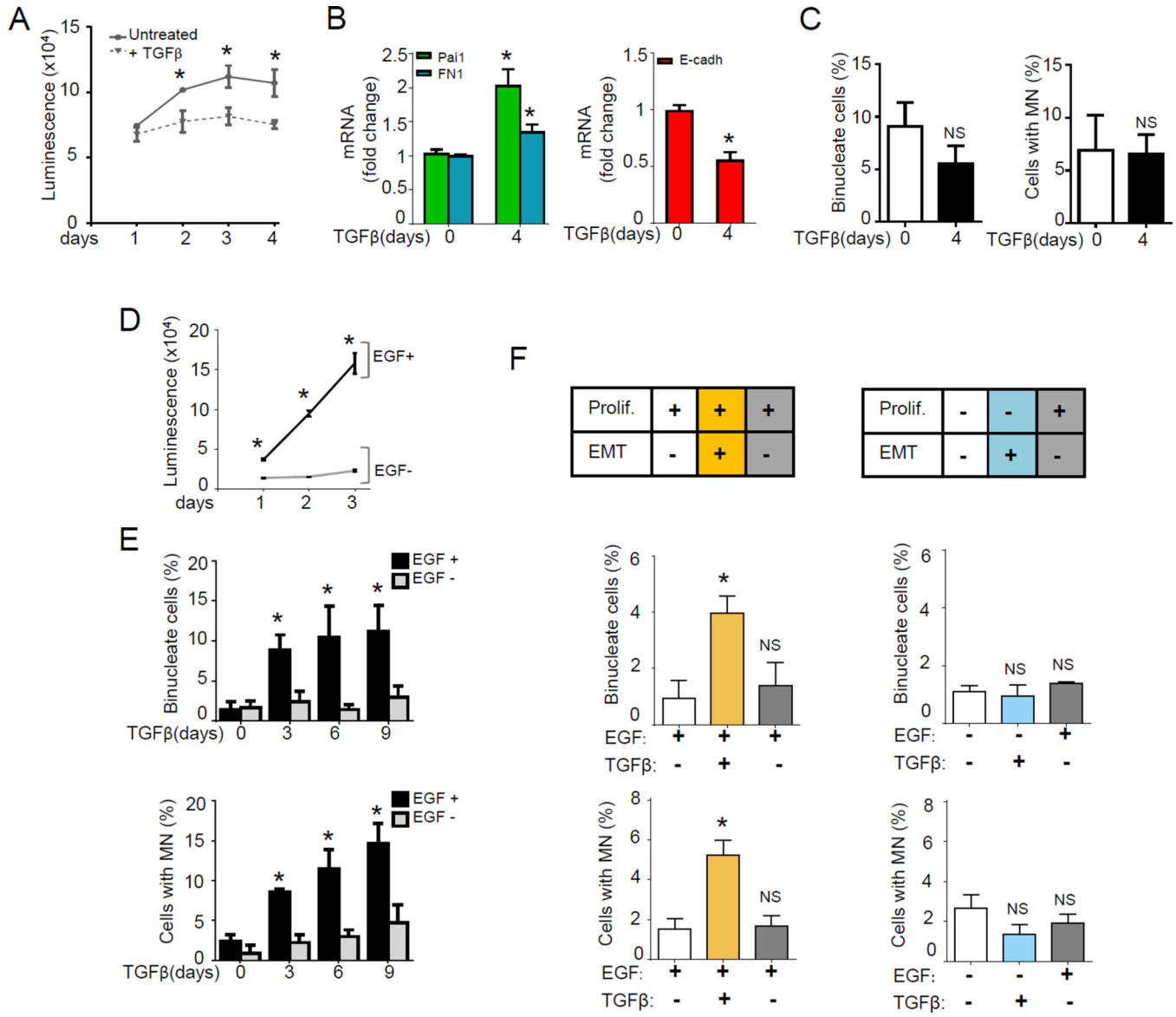

Figure 3. TGFβ-induced mitotic anomalies are dependent on cell proliferation during EMT

A) TGFβ inhibits the proliferation of freshly isolated normal mouse mammary epithelial cells (nMMECs).

B) EMT marker expression in TGFβ-treated nMMECs.

C) Percentage of BN and MN containing cells in untreated and TGFβ-treated nMMEC cultures. Data represent mean ± s.d. derived from two independent experiments. NS: not significant.

D) Proliferation of MCF10A cells grown in medium with and without EGF. *p<0.001

E) TGFβ-mediated mitotic aberrations require proliferation. Quantification of BN and MN cells in cultures grown with or without EGF ± 5ng/mL TGFβ. Data represent mean ± s.d. derived from two independent experiments. *p<0.01.

F) Left: TGFβ was added to proliferating cells grown in the presence of EGF followed by removal of TGFβ. BN and MN cells were quantified. The table above indicates the

corresponding proliferative and EMT status of cells for each condition shown in the graph. The condition in which the cells are proliferating while undergoing EMT is highlighted in yellow. Right panels: TGFβ was added to non-proliferating MCF10A cells grown in the absence of EGF followed by removal of TGFβ and addition of EGF. BN and MN cells were quantified. Table above indicates the corresponding proliferative and EMT status of cells for each condition shown in the bar graph. The graphs shown (mean ± s.d.) are representative of two independent experiments. *$p<0.01$; NS: not significant.

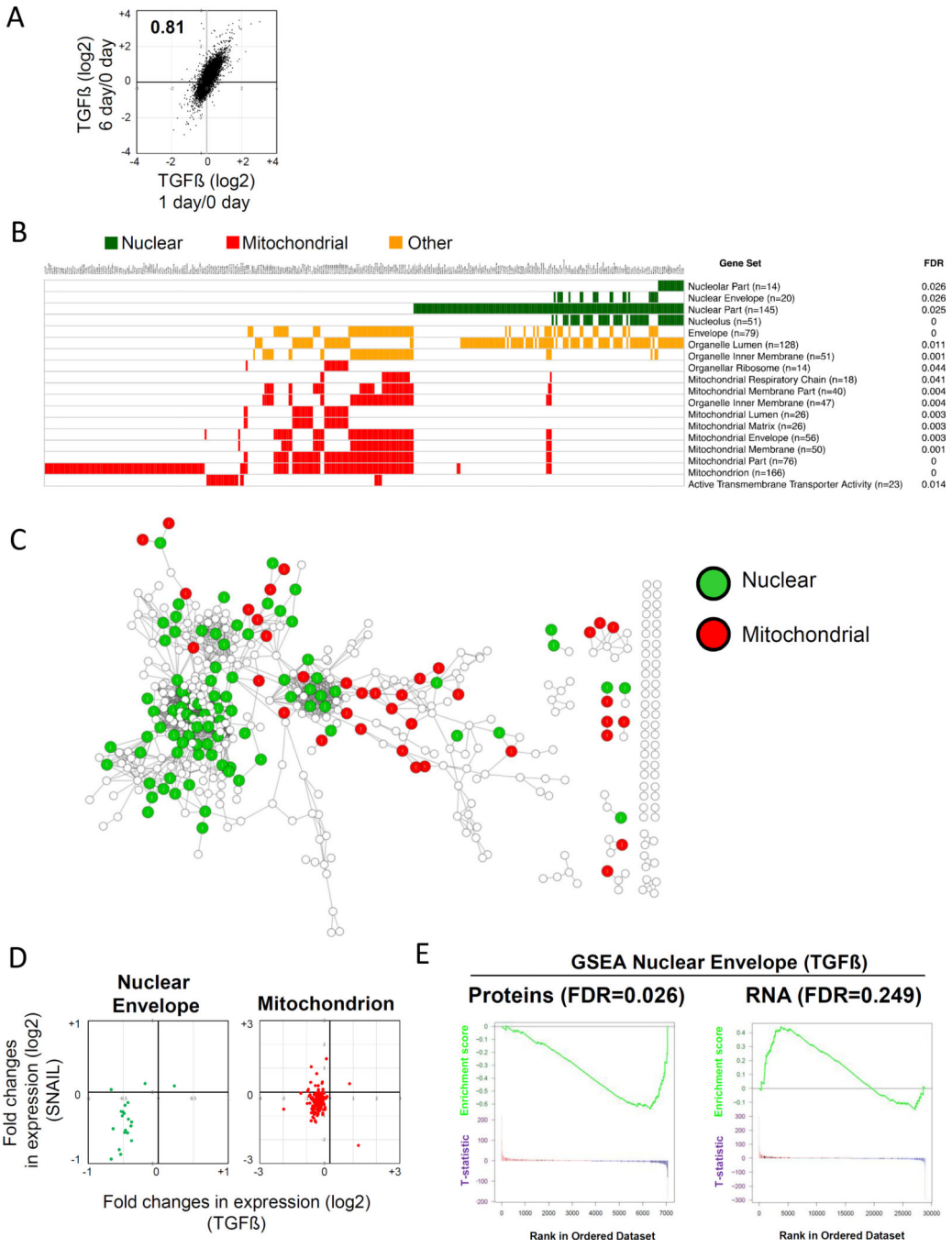

Figure 4. TGFβ and SNAIL suppress nuclear envelope (NE) and nuclear pore complex proteins

A) Proteins differentially expressed in 1 and 6 day TGFβ-treated samples compared to untreated controls show significant correlation (n=2 for each condition).

B) Gene set enrichment analysis (GSEA) of proteins suppressed by TGFβ [(False discovery rate (FDR) ≤0.05)]. Genes contributing to nuclear, mitochondrial and organelle architecture (other) are highlighted in green, red and orange, respectively. The number of core enrichment genes of each gene set is given in parentheses. See Gene list in Database 1.

C) Cytoscape network maps depicting NE, nucleolus and mitochondrial proteins suppressed by TGFβ (High confidence score > 0.70). Red and green circles represent individual TGFβ-suppressed mitochondrial and nuclear proteins (NE and Nucleolus genesets) within the enriched GSEA pathways (FDR≤0.05).

D) NE and mitochondrial proteins suppressed by TGFβ are also suppressed in MCF10A cells following SNAIL induction. Each dot on the plot represents a single protein belonging to the category shown. Also see Fig. S5E.

E) GSEA analyses of RNA and proteins altered by TGFβ show that TGFβ-mediated suppression of the NE components occurs only at the proteomic level.

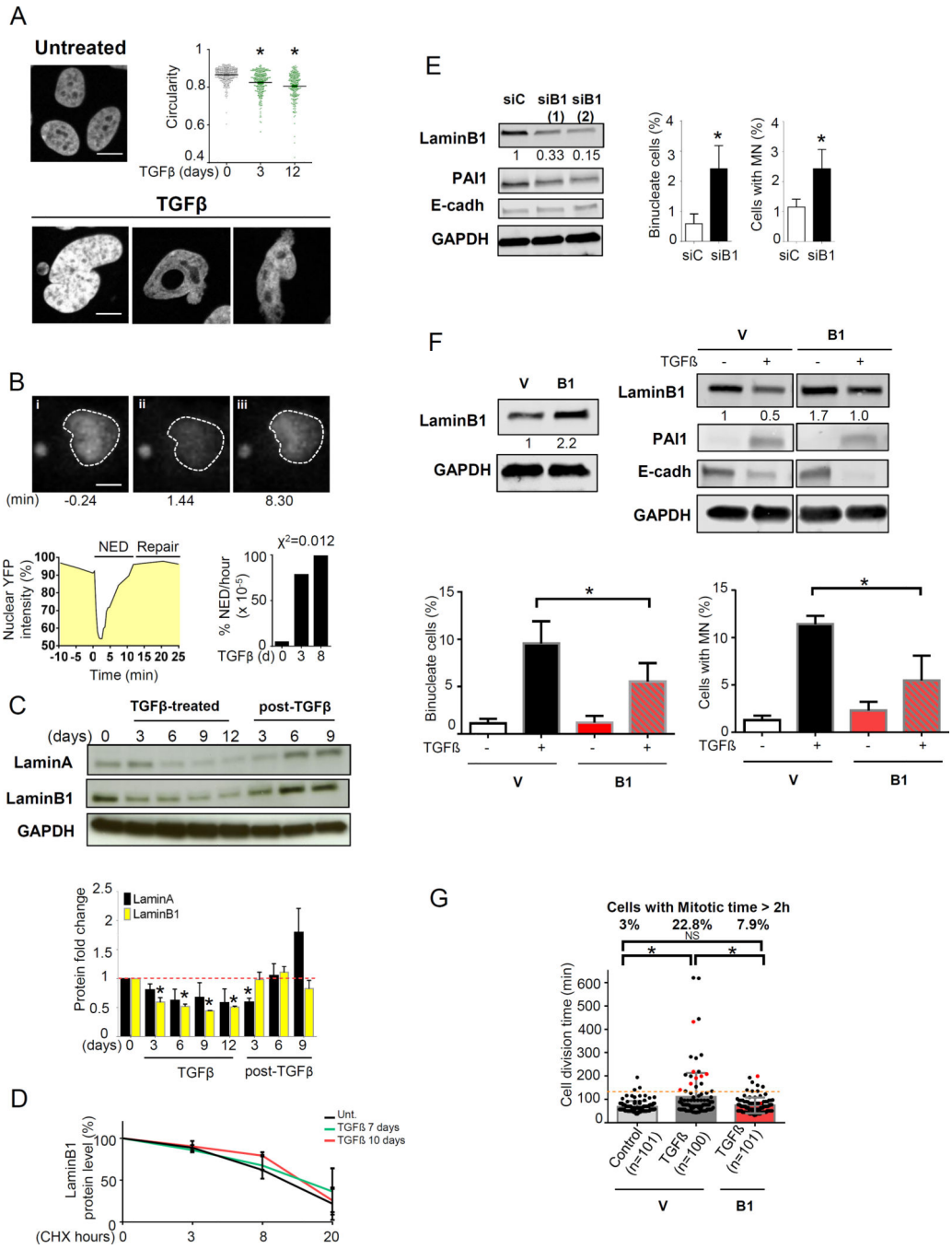

Figure 5. TGFβ induces NE disruption, and modulation of LaminB1 phenocopies TGFβ-induced mitotic defects

A) DAPI stained nuclei of cells show that TGFβ induces nuclear blebbing and decreases nuclear circularity.

B) TGFβ induces NE disruption (NED) during interphase. Localization of YFP-tagged nuclear localization signal (NLS) of the SV40 large T antigen in the nucleus (i), its disappearance through NED (ii), and its reappearance in the nucleus following NE repair (iii) is shown in a TGFβ-treated cell at interphase. Graph shows fluorescence intensity

changes in the nucleus of the above cell over time. Graph shows the percentages of untreated and TGFβ-treated cells exhibiting NED per hour (χ^2 test =0.012).

C) TGFβ suppresses LaminA and B1 proteins in MCF10A cells. Graphs show fold changes in LaminA and B1 proteins following TGFβ treatment and its withdrawal. Data represents mean ± SD from 3 independent experiments. *p<0.05.

D) Suppression of LaminB1 protein by TGFβ is not due to decreased protein stability. LaminB1 protein expression in MCF10A cells treated with cycloheximide (CHX) ± TGFβ.

E) Knockdown of LaminB1 leads to mitotic abnormalities. LaminB1 was suppressed in MCF10A cells using two pools of siRNA [siB1 (1) and siB1 (2)]. Western blot shows that suppression of LaminB1 does not change EMT markers. Graphs show the percentages of BN and MN cells in control and si-LaminB1 cells. siB1 represents the mean± SD derived from cells transfected with siB1 (1) and siB1(2).

F) Ectopic expression of LaminB1 partially rescues TGFβ-mediated mitotic abnormalities. Upper Left: LaminB1 protein expression in MCF10A cells infected with LaminB1 (B1) expressing lentiviral construct. Vector (V) control is shown. Upper Right: LaminB1 and EMT marker expression in TGFβ-treated Vector alone and LaminB1 (B1) overexpressing cells. Quantification of band intensities is shown below. Note that TGFβ suppresses LaminB1 protein in B1 overexpressing cells as well, but to a level observed in untreated vector control. Lower: Graphs show percentages of BN and MN cells in TGFβ-treated Vector (V) and LaminB1 (B1) overexpressing cells. Data represent mean± SD from five independent experiments. G) Cell division time of TGFβ-treated vector (V) and LaminB1 (B1) expressing cells. The number of cells analyzed for each condition and the fraction of cells with mitotic time >2 hours in each sample are shown. Red dots denote mitosis with cytokinesis failure. *p<0.0001. NS: nonsignificant.

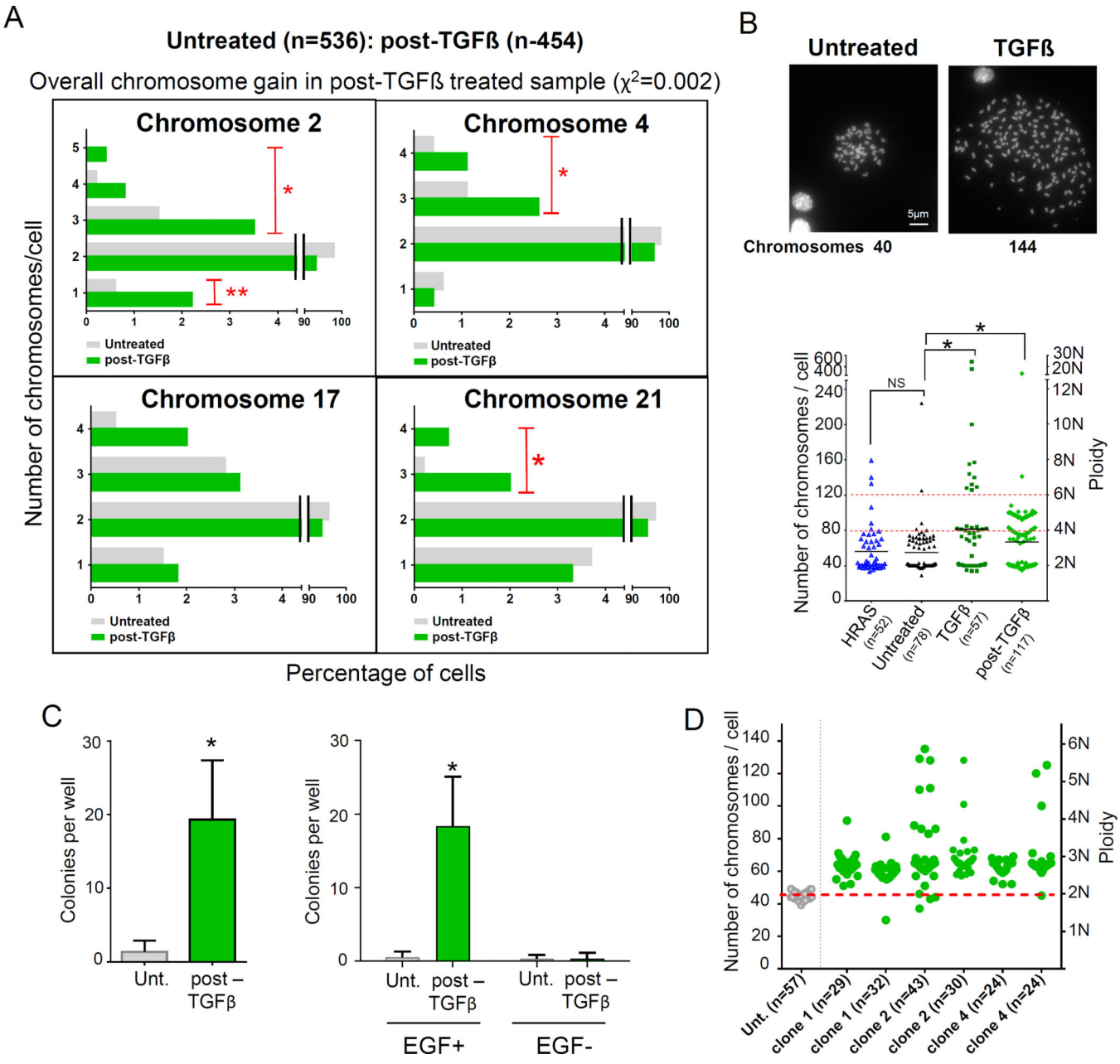

Figure 6. TGFβ induces aneuploidy and tumorigenic phenotypes

A) MCF10A cells were treated with TGFβ for 12 days followed by TGFβ withdrawal for 12 days (post-TGFβ), which reverses EMT (Mesenchymal to Epithelial Transition-MET; Fig. 2A). Cells were analyzed by interphase DNA-FISH against chromosomes 2, 4, 17 and 21. Graphs show percentages of untreated (n=538) and post-TGFβ-treated MCF10A cells (n=454) exhibiting mono, di, tri, tetra and pentasomy for each of the chromosomes. There is significant gain of chromosomes 2 (* X^2=0.002), 4 (* X^2=0.025) and 21 (* X^2 =0.0007), and a significant loss of chromosome 2 (** X^2 = 0.02). The overall gain of chromosomes in cells with a history of TGFβ exposure is highly significant (X^2=0.0002).

B) TGFβ induces Aneuploidy/polyploidy in CDβgeo cells. CDβgeo cells were treated with TGFβ for 14 days followed by TGFβ withdrawal for 24 days. Upper: Aneuploid/polyploid cell in TGFβ-exposed CDβgeo cultures. An untreated cell is shown as control. Total number of chromosomes in each cell is shown. Lower: Plot shows chromosome number in each cell and the number of cells analyzed for each condition. Untreated and HRAS expressing CDβgeo cells are shown as controls. *$p<0.01$.

C) TGFβ induces growth in soft agar. Left: MCF10A cells treated with TGFβ for 12 days followed by TGFβ withdrawal for 9 days were grown in soft agar for 4 weeks (without TGFβ). Right: MCF10A cells grown with or without EGF were treated with TGFβ for 6 days followed by TGFβ withdrawal for 3 days and seeded in soft agar (without TGFβ). Untreated MCF10A cells were used as control. Data represent mean of colony numbers ± s.d of three (left) and six (right) experiments, respectively; *$p<0.05$.

D) Proliferating MCF10A cells exposed to TGFβ and selected for soft agar growth are highly tumorigenic and enriched for a population of aneuploid/polyploid cells. Three colonies, established following soft agar growth, and injected into mice form tumors (n=2 mice per clone, Figure S8F). The tumors were removed, cultured in vitro and chromosomes were counted following metaphase spread. Plot shows the number of chromosomes per cell and the number of cells analyzed from each individual clone.

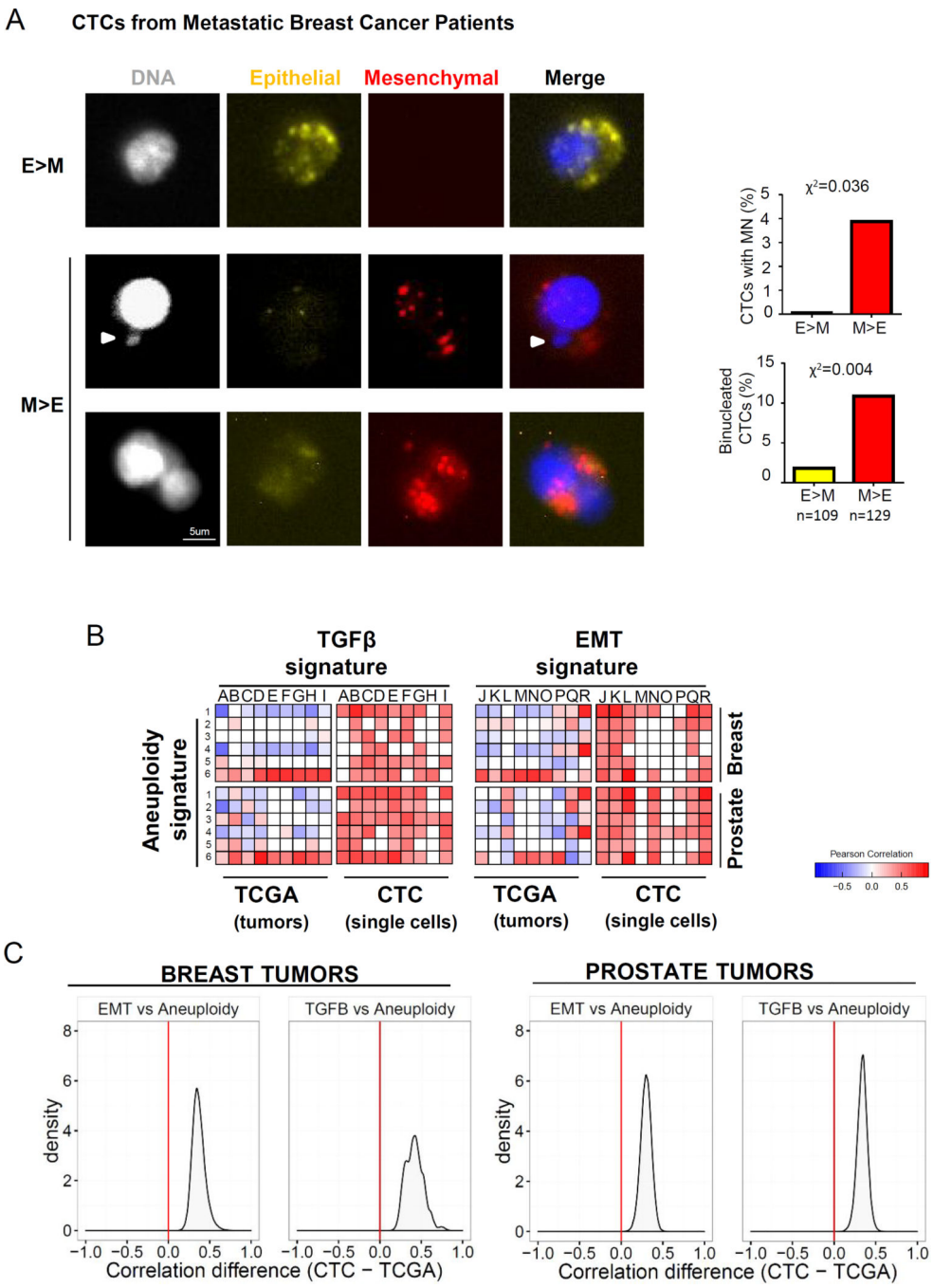

Figure 7. Mesenchymal CTCs from metastatic breast cancer patients exhibit genomic instability

A) CTCs from metastatic breast cancer patients were stained by RNA-ISH using probes against epithelial (E: CDH1, EPCAM, KRT5, 7, 8, 18, 19; yellow dots) and mesenchymal (M: FN1, CDH2, PAI1; red dots) markers (Yu et al., 2013). Representative images of CTCs expressing E>M markers (upper), and CTCs expressing M>E markers harboring MN (middle, arrowhead) and BN (lower) are shown. Graph shows the percentage of BN and MN harboring CTCs expressing E>M (n=109) and M>E (n=129) markers. Scale bar, 5 μM.

B) TGFβ and EMT signatures correlate with Aneuploidy metagene signatures in human breast and prostate tumor cells. Heat maps showing the Pearson correlation between each of the nine TGFβ, nine EMT signatures, and the six aneuploid metagene signatures in TCGA breast and prostate cancer data sets and in RNASeq data from CTCs derived from breast and prostate cancer patients (Aceto et al., 2014; Miyamoto et al., 2015). The gene sets used in the correlation analysis (TGFβ signatures: A-I, EMT signatures: J-R, Aneuploidy signatures: 1–6) are shown in Table S2. Correlations shown have a FDR < 0.1.

C) Probability density plots of the bootstrap test statistic (CTC – TCGA) with respect to aneuploidy signature correlations in breast and prostate tumor samples. TGFβ and EMT signatures are more strongly correlated with aneuploid signatures in pure populations of CTCs and single CTCs derived from breast and prostate cancer patients, respectively, compared with TCGA dataset from breast and prostate cancer patients (vertical red bar indicates correlation difference of zero). The permutation bootstrap p-value is provided for each density plot ($p<0.05$ are significant).